

RESEARCH ARTICLE

Tau-neurodegeneration *mismatch* reveals vulnerability and resilience to comorbidities in Alzheimer's continuum

Xueying Lyu¹ | Michael Tran Duong¹ | Long Xie² | Robin de Flores³ |
Hayley Richardson⁴ | Gyujoon Hwang² | Laura E. M. Wisse⁵ | Michael DiCalogero⁶ |
Corey T. McMillan⁶ | John L. Robinson⁷ | Sharon X. Xie⁴ | Edward B. Lee⁷ |
David J. Irwin⁶ | Bradford C. Dickerson⁸ | Christos Davatzikos¹ | Ilya M. Nasrallah² |
Paul A. Yushkevich² | David A. Wolk⁶ | Sandhitsu R. Das⁶ | for the Alzheimer's Disease
Neuroimaging Initiative

¹Departments of Bioengineering, University of Pennsylvania, Philadelphia, Pennsylvania, USA

²Departments of Radiology, University of Pennsylvania, Philadelphia, Pennsylvania, USA

³Université de Caen Normandie, INSERM UMRS U1237, Caen, France

⁴Department of Biostatistics, Epidemiology and Informatics, University of Pennsylvania, Philadelphia, Pennsylvania, USA

⁵Department of Clinical Sciences Lund, Lund University, Lund, Sweden

⁶Departments of Neurology, University of Pennsylvania, Philadelphia, Pennsylvania, USA

⁷Departments of Pathology and Laboratory Medicine, University of Pennsylvania, Philadelphia, Pennsylvania, USA

⁸Massachusetts General Hospital, Boston, Massachusetts, USA

Correspondence

David A. Wolk and Sandhitsu R. Das, 3701
Hamilton Walk, Philadelphia, PA, 19104, USA.
Email: David.Wolk@penncmedicine.upenn.edu
and sudas@penncmedicine.upenn.edu

Data used in preparation of this article were obtained from the Alzheimer's Disease Neuroimaging Initiative (ADNI) database (adni.loni.usc.edu). As such, the investigators within the ADNI contributed to the design and implementation of ADNI and/or provided data but did not participate in analysis or writing of this report. A complete listing of ADNI investigators can be found at: http://adni.loni.usc.edu/wp-content/uploads/how_to_apply/ADNI_Acknowledgement_List.pdf

Funding information

Alzheimer's Disease Neuroimaging Initiative; National Institutes of Health, Grant/Award Number: U01 AG024904; DOD ADNI, Grant/Award Number: W81XWH-12-2-0012;

Abstract

INTRODUCTION: Variability in relationship of tau-based neurofibrillary tangles (T) and neurodegeneration (N) in Alzheimer's disease (AD) arises from non-specific nature of N, modulated by non-AD co-pathologies, age-related changes, and resilience factors.

METHODS: We used regional T-N residual patterns to partition 184 patients within the Alzheimer's continuum into data-driven groups. These were compared with groups from 159 non-AD (amyloid "negative") patients partitioned using cortical thickness, and groups in 98 patients with *ante mortem* MRI and *post mortem* tissue for measuring N and T, respectively. We applied the initial T-N residual model to classify 71 patients in an independent cohort into predefined groups.

RESULTS: AD groups displayed spatial T-N *mismatch* patterns resembling neurodegeneration patterns in non-AD groups, similarly associated with non-AD factors and diverging cognitive outcomes. In the autopsy cohort, limbic T-N mismatch correlated with TDP-43 co-pathology.

DISCUSSION: T-N *mismatch* may provide a personalized approach for determining non-AD factors associated with resilience/vulnerability in AD.

This is an open access article under the terms of the [Creative Commons Attribution-NonCommercial](https://creativecommons.org/licenses/by-nc/4.0/) License, which permits use, distribution and reproduction in any medium, provided the original work is properly cited and is not used for commercial purposes.

© 2023 The Authors. *Alzheimer's & Dementia* published by Wiley Periodicals LLC on behalf of Alzheimer's Association.

National Institute on Aging, Grant/Award Numbers: R01 AG056014, RF1 AG069474, P01AG066597, P30AG072979, U19AG062418; National Institute of Biomedical Imaging and Bioengineering

KEYWORDS

aging, Alzheimer's disease, co-pathologies, multi-modality imaging, neurodegeneration, *post mortem*, tau

1 | BACKGROUND

Alzheimer's disease (AD) is heterogenous in age of onset, course, cognitive phenotype, and presence of underlying co-pathology.¹⁻⁴ In particular, concomitant pathologies are frequently present in individuals with AD, such as cerebrovascular disease and/or other degenerative pathologies, including TAR DNA-binding protein 43 (TDP-43) and alpha-synuclein proteinopathies.^{2,3,5,6} Alzheimer's also occurs in the context of an aging brain with variability in age-related changes (accelerated vs. decelerated) that also may influence clinical presentation and rate of decline.⁷ Finally, resilience factors may affect outcomes and degree of pathology.⁸⁻¹¹ This heterogeneity, along with lack of well-validated markers of non-AD influences, poses a substantial challenge for application of AD targeting therapeutics. As we enter an era of disease-modifying therapies, debate remains about who might benefit most from these interventions and to what extent specifically targeting AD-related pathology can be expected to slow decline in the context of co-pathologies. A precision medicine approach that quantifies the contribution of AD-related pathology to neurodegeneration in a dissociable manner from non-AD factors is essential as therapies move into practice and for stratification in intervention studies.

The accumulation of amyloid plaques (A β) and tau neurofibrillary tangles (NFT) are the two hallmark pathological features of AD. *Post mortem* studies¹²⁻¹⁴ and PET imaging have supported the hypothesis that NFTs are more tightly linked to downstream neurodegeneration than amyloid plaques.¹⁵⁻¹⁹ Thus, expected neurodegeneration *due to* AD may be largely explained by the local presence and amount of tau pathology.

We exploit the non-specific nature of neurodegeneration to account for non-AD processes by quantifying the degree and spatial pattern of deviation from the expected level of N (neurodegeneration) for a given level of T (tau). In essence, we “regress out” the effects of AD on brain structure which should reveal patterns of relative atrophy associated with non-AD factors. These regional patterns of T-N discordance may uncover groups associated with specific potential co-pathologies (e.g., greater medial temporal atrophy with concomitant TDP-43) and/or types of resilience. We hypothesized that “vulnerable” groups with more N than expected for T would likely be associated with non-AD pathologies. Conversely, “resilient” groups may be associated with protective factors, including greater brain reserve, such that they have less N than expected for T.

The current analysis extends our prior work²⁰ using this approach, which we also explored using a metabolic²¹ measure of neurodegeneration. We previously found meaningful associations between T-N *mismatch* and several factors, including age, white matter hyperintensity (WMH) burden and cognition. However, specific links to non-AD

drivers of regional T-N mismatch were limited and require additional studies.

In this manuscript, we take further steps to understand and validate T-N mismatch in both in vivo and ex vivo analyses. (1) If T-N mismatch reflects neurodegeneration due to non-AD factors after AD effects are “regressed out”, then we expect patterns of mismatch would overlap with patterns of atrophy in patients with cognitive impairment due to non-AD etiologies. To test this hypothesis, we compared T-N mismatch patterns in patients with AD (amyloid positive/A+) with patterns of cortical thickness in those without AD (amyloid negative/A-). (2) In addition to overlapping spatial patterns between these two groups, we predicted overlapping associations with surrogates of non-AD factors (e.g., WMH) that may drive non-AD neurodegeneration in T-N mismatch and the corresponding non-AD groups (A-) defined above. (3) Brain age itself is conceptualized as one potential non-AD factor beyond specific co-pathologies that can convey brain reserve or vulnerability and was operationalized using a machine learning-based metric that was developed to reflect brain changes orthogonalized from AD.⁷ (4) Links to specific co-pathologies with T-N mismatch were further explored in an autopsy sample with *ante mortem* imaging. (5) Given comorbidities may synergistically interact with AD and contribute to cognitive impairment, we predicted that “vulnerable” versus “resilient” T-N groups would also differ in longitudinal cognitive decline. (6) Finally, to evaluate the potential feasibility of this approach on individual classification in the spirit of “precision medicine”, we determined group membership of individuals in an independent cohort using the model developed in the initial in vivo analysis.

2 | METHODS

2.1 | Participants

2.1.1 | ADNI dataset

We included 343 participants from the Alzheimer's Disease Neuroimaging Initiative (ADNI) dataset (<http://adni.loni.usc.edu>) who were classified with a diagnosis of mild cognitive impairment (MCI) or dementia. All participants had to have both a Tau positron emission tomography (PET) scan and T1-weighted MRI scan. The closest MRI to tau PET scans were selected. The average time between tau scan and MRI scan was 14.4 (\pm 10) (SD) months. There were 184 amyloid positive (A+) and 159 amyloid negative (A-) patients included in this study. Most of the A+ patients were also in our prior study.²⁰ The summarized clinical characteristics of the cohort are reported in Table S1. In addition, we included 137 A- cognitively unimpaired adults from ADNI as controls in the voxel-wise thickness comparison analysis (Table S1).

2.1.2 | AVID dataset

We included 71 A+ symptomatic patients (36 female and 35 male) with a pair of Tau PET scan and T1-weighted MRI scans from the Avid Radio-pharmaceuticals' study (A05) with inclusion criteria for age ≥ 50 and Mini-Mental State Examination (MMSE) score > 10 .²² Participants provided written informed consent and both informed consent and the protocol were approved by the relevant Institutional Review Boards.²² The Tau PET scan and T1-weighted MRI scan for each patient was obtained from the same visit. All participants were symptomatic, including 29 with dementia-level impairment and 42 with MCI. Average age was 73.6 ± 9.8 , and average MMSE score was 24.7 ± 4.3 . The summarized clinical characteristics of this cohort is displayed in Table S2.

2.1.3 | Dataset

We included 98 autopsies (age 71.7 ± 11 years at MRI scan and age 75.1 ± 11 years at death) from the University of Pennsylvania Center for Neurodegenerative Disease Research (CNDR). All individuals had an *ante mortem* research-quality T1-weighted (T1w) MRI scan. For those with multiple scans, the closest to death was chosen. Inclusion also required that individuals had a Consortium to Establish a Registry for Alzheimer's Disease (CERAD) score of ≥ 2 , as that reflects a threshold for detection of amyloid positivity with PET.²³ Outside of the CERAD cutoff criteria, we broadly accepted a range of additional pathologies and phenotypes. The majority were symptomatic (10 MCI and 85 dementia) while 3 cases were cognitively unimpaired. Of the 98 cases, 75 had intermediate/high Alzheimer's disease neuropathologic change (ADNC)²⁴ as primary diagnosis (12 cases had high/intermediate ADNC, but not as primary). In the other 23 cases, 14 had DLB as primary, 6 had a non-AD tauopathy as primary, 2 had FTL/ALS TDP-43 as primary, and 1 had CVD as primary. Semi-quantitative regional tau severity was determined by histology. The average time interval between MRI scan date and autopsy date was $46.0 (\pm 31)$ months. All procedures during life were performed with prior informed consent in accordance with Penn Institutional Review Board guidelines.

Given that not all cases above had intermediate or high ADNC, we performed a secondary analysis that required its presence instead of the CERAD criteria. In total, 94 intermediate/high ADNC cases were included in this analysis. The overall goal of these analyses was to include cases with AD pathology and determine the degree to which our mismatch metric captures the presence of co-pathologies.

2.2 | Image acquisition and processing

2.2.1 | Image acquisition

For both ADNI and AVID cohorts, we processed both T1-weighted MRI and tau PET (¹⁸F-flortaucipir) scans to obtain cortical thickness and tau SUVR for 100 bilateral gray matter regions of interest

RESEARCH IN CONTEXT

- 1. Systematic reviews:** Although there is a relatively close relationship between tau (T) and neurodegeneration (N), the variability of T-N relationships may reveal potential factors outside of Alzheimer's disease (AD). We previously introduced the T-N *mismatch* data-driven framework. Nevertheless, the understandings of specific links to non-AD drivers of regional T-N *mismatch* were limited. Further investigations into its utilization are required for its potential applications in clinical settings.
- 2. Interpretation:** This work further explored the concept of how T-N *mismatch* reveals vulnerability and resilience through both in vivo and ex vivo studies. We found evidence that distinct T-N phenotypes were associated with specific non-AD modulators, which predicted future clinical outcomes. Furthermore, we evaluated the potential application of this approach on individual classification in the spirit of "precision medicine".
- 3. Future directions:** Our findings validated and extended the understanding of T-N dissociations. Alternative approaches of modeling T-N *mismatch* could constitute future directions to further investigate this concept.

(ROIs). The detailed image acquisition and processing methods have been previously described.²⁰ In brief, the T1w MRI scan of resolution $1.0 \times 1.0 \times 1.0 \text{ mm}^3$ were acquired by ADNI, while PET images were of variable resolution, but reprocessed to a similar 0.8 cm full-width at half maximum resolution. FLAIR MRI was acquired in the same session as T1w MRI with variable spatial resolution as prescribed in the ADNI protocol. For the CNDR dataset, *ante mortem* T1-weighted structural MRI scan for all subjects were obtained with resolution ranging from $0.5 \times 0.5 \times 1 \text{ mm}^3$ to $1.25 \times 1.25 \times 1.20 \text{ mm}^3$. For AVID dataset, the MRI scans have resolution $1.0 \times 1.0 \times 1.2 \text{ mm}^3$.

2.2.2 | T1-MRI processing

The image processing methods have been described in our prior work.²⁰ Briefly, the T1-weighted MRI was processed with the ANTs cortical thickness pipeline²⁵ which includes steps for intensity inhomogeneity correction and tissue segmentation. The MRI scans were parcellated into cerebellar, cortical, and subcortical ROIs using a multi-atlas segmentation method.²⁶ The volumetric thickness map for each subject was estimated via DiReCT cortical thickness estimation method²⁷ to generate volumetric thickness maps. ROI-based thickness was calculated by averaging the thickness maps across voxels within the gray matter ROIs. The same processing for T1-weighted MRI was applied to ADNI, AVID, and CNDR cohorts.

2.2.3 | PET processing

ADNI provides post-processed PET images that are generated by averaging co-registered individual frames. Post-processed PET images were registered to participants' T1-weighted structural MRI using ANTs.²⁸ The following ANTs parameters were used. Metric: Mattes mutual information (weight = 1, number of bins = 32), Transformation model: Rigid (gradient step = 0.2, Smoothing levels = $4 \times 2 \times 0$, Shrink factor = $4 \times 2 \times 1$). MRI parcellated ROIs were transferred to PET space. Mean PET tracer uptake in cerebellar gray matter (¹⁸F-Flortaucipir) or cerebellar gray and white matter (¹⁸F-Florbetapir or ¹⁸F-Florbetaben) was used as a reference region to generate a standardized uptake value ratio (SUVR) map for each participant.

We additionally processed amyloid PET scans (18F-florbetaben or ¹⁸F-florbetapir tracer) for determining amyloid status. Amyloid status was determined by using a composite ROI measure of ¹⁸F-florbetaben or ¹⁸F-florbetapir tracer uptake.²⁹ As previously published,²⁰ we used an SUVR ≥ 1.11 ⁴¹ for ¹⁸F-Flortaucipir and ≥ 1.08 for ¹⁸F-Florbetaben to define a positive amyloid scan (A+).

We processed ¹⁸F-Flortaucipir PET for AVID dataset. Attenuation-corrected image frames were first motion-corrected by MCFLIRT³⁰ with 6 degree of freedom correction and averaged. The post-processed PET images were then processed following the same method as the ADNI cohort to get regional SUVR.

2.2.4 | White matter hyperintensity processing

The WMHs were segmented from FLAIR images using a deep learning-based method³¹ that was a top performer in a WMH segmentation challenge.

2.3 | Post mortem neuropathology measurement

All autopsies at the Penn CNDR were conducted with detailed procedures described elsewhere,³² including routine examination of up to sixteen regions³² and uniform immunohistochemistry analyses. Briefly, the tissue was embedded in paraffin block, cut into 6 μm sections, and immunostained for a variety of proteins in specific regions. Antibody NAB228 was used to target amyloid deposits, PHF-1 to measure phosphorylated tau deposits and pS409/410 to detect phosphorylated TDP-43 deposits. The neuropathology burden of each region was then evaluated by pathologists by assigning a semi-quantitative score of none (0), rare (0.5), mild (1), moderate (2), or severe (3). The diagnosis of the degree of ADNC was determined by standard criteria.²⁴

2.4 | Modeling T and N mismatch and clustering

2.4.1 | A + ADNI T-N mismatch clustering

The T and N relationship was modeled by robust linear regression between regional tau SUVR and cortical thickness, respectively. The bi-square weighting function was used to mitigate the effect of outliers.

A natural log transformation was applied on tau SUVR as the independent variable to mitigate the effects of potentially skewed SUVR distribution. The regression residuals were discretized into a ternary variable based on whether they were more than 1.5 standard deviations above (+1) or below (−1) the regression line, or neither (0). We used 1.5 standard deviation as the threshold to define "outliers". In our prior work,²⁰ this threshold resulted in highly overlapping clusters compared to other thresholds or no threshold at all. These ternary variables obtained from 100 bilateral ROIs were entered into Ward's D2 hierarchical clustering³³ to generate data-driven grouping of subjects. The number of groups was determined by the elbow³⁴ method which visualizes within-group similarity and the dendrogram structure which visualizes between-group distances (Figure S1A). The latter proved more useful than the former in choosing the number of groups. Consideration of group size such that every group had a reasonable number of participants and number of groups in our prior work²⁰ also influenced decisions on choosing the cut point in the dendrogram structure. The three-dimensional regional mean residual map was visualized using MRICroGL.³⁵

2.4.2 | A− ADNI thickness z-score clustering

The thickness of A− patients was standardized into z-scores referenced to 137 cognitively normal individuals for all 100 gray matter regions. Each regional z-score thickness was discretized into ternary variables based on 1.5 standard deviations similar to the A+ T-N clustering. These ternary variables obtained from 100 bilateral ROIs were entered into Ward's D2 hierarchical clustering³³ to obtain N_z groups in the same manner as above (Figure S1B). Through qualitative visual assessment, we found matching groups across the A− N_z and A+ T-N clusters. To quantitatively assess the degree of matching, we measured the Euclidean distance between each A− N_z individual's discretized regional thickness z-score with the average discretized regional T-N residual of each of the T-N groups. Moreover, we assessed the similarity of spatial patterns in Figure 1A by computing a Pearson correlation between two 400-element vectors: one comprising mean thickness z-scores of all 100 ROIs for the 4 N_z groups (as visualized in Figure 1A right), and the other comprising mean T-N residuals for the corresponding T-N groups (as visualized in Figure 1A left). This was compared with the correlation for all possible pairwise group mappings.

2.4.3 | A + AVID T-N mismatch testing

The regional T-N residuals of the AVID cohort were obtained from the regional T-N regression models built from the ADNI A+ cohort. Regional residuals were discretized based on the 1.5 standard deviation of residuals from the training set regression (ADNI). The Euclidean distance between each AVID patient's discretized vector and the averaged discretized residual vector of each T-N group from the ADNI cohort was obtained and compared. Group identity was determined by

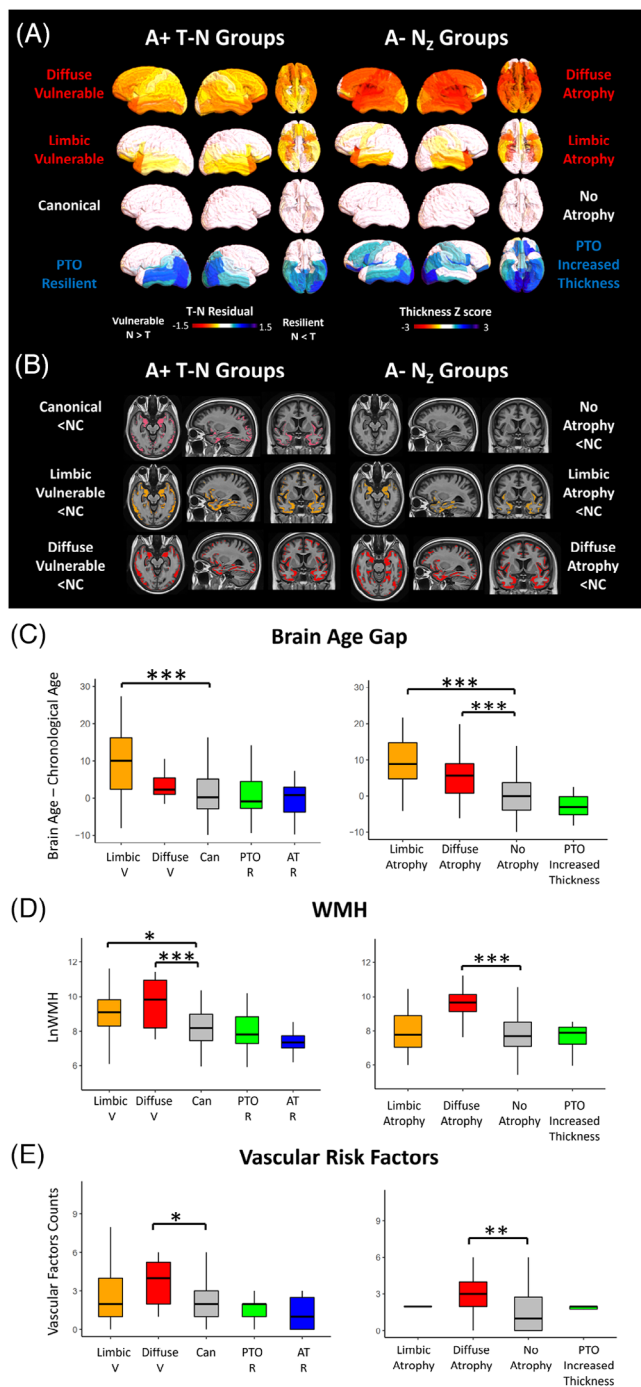


FIGURE 1 T-N groups resembled N_2 groups and were associated with non-AD modulators in ADNI cohort. (A) The T-N residual patterns for T-N groups were similar to regional thickness z-score patterns for identified groups among A- patients from ADNI by clustering on standardized thickness using 137 normal individuals: No atrophy (close to 0 z-score), atrophy (negative z-score), increased thickness (positive z-score). (B) Voxel-wise analyses reveal significantly less thickness of T-N groups (left) and N_2 groups compared with cognitively unimpaired control (NC, $N = 137$) controlling for age and sex ($P_{FWER} < 0.05$). The colored areas represent significant difference with the cognitively unimpaired control for each group. (C) The between-group brain age gap (brain age - chronological age) pair-wise comparison for T-N groups (left) and N_2 groups (right) after covarying by age. (D) The between-group white matter

finding the shortest Euclidean distance among all six of the original A+ T-N groups.

2.4.4 | Ex vivo T-N mismatch clustering

To validate T-N *mismatch* on ex vivo autopsies, we used cortical thickness measured from *ante mortem* MRI and regional tau burden measured from histological staining for modeling T-N *mismatch*. Among all 16 regions, only six cortical ROIs had consistent tau measurement available: anterior cingulate gyrus, entorhinal cortex, angular gyrus plus middle occipital gyrus, middle frontal gyrus, superior temporal gyrus, and amygdala. The T-N relationships were modeled following a procedure similar to the in vivo analysis, except that we additionally included the time between MRI scan date and autopsy date as covariate for modeling. The independent variable of tau burden was treated as a continuous variable rather than as a factor here since it resulted in lower Akaike information criterion (AIC),³⁶ indicating better model fit, for all six regions. The same clustering procedure that was used for the in vivo data, as well as metrics of spatial overlap, was then performed on obtained residuals to partition subjects (Figure S1C).

2.5 | ADNI comorbidities evaluation

Vascular risk factors data were obtained from the ADNI INITHEALTH table. Factors counted as vascular risk factors include hypertension, hyperlipidemia, type II diabetes, arrhythmia, cerebrovascular disease, endovascular management of head/neck vessels, coronary artery disease, coronary interventions, heart failure, structural heart defects/repair, peripheral artery disease, and smoking. The number of vascular risk factor for each patient was counted.

Brain age was obtained by the machine-learning based Spatial Pattern of Atrophy for Recognition of Alzheimer's Disease (SPARE) models.⁷ It uses MRI scans to infer a measure of brain age that is specifically formulated to be orthogonal to AD-related brain changes. The

hyperintensities volume comparison with age as covariates among T-N groups (left) and N_2 (right) groups. (E) The pair-wise comparisons of vascular risk factors for T-N groups (left) and N_2 groups (right). The count of vascular risk factors is the sum of participant risk factors, assayed categorically, for hypertension, hyperlipidemia, type II diabetes, arrhythmia, cerebrovascular disease, endovascular management of head/neck vessels, coronary artery disease, coronary interventions, heart failure, structural heart defects/repair, peripheral artery disease, and smoking. The mixed group was excluded in the analyses of T-N groups comparison due to its small size. For C-E, pairwise comparisons between groups were performed. Only significant comparisons with the typical groups (canonical for T-N groups, no atrophy group for N_2 groups), respectively, were marked in the figures. Significant levels corrected by Bonferroni multiple comparison are denoted as $*p < 0.05$, $**p < 0.01$, $***p < 0.001$.

TABLE 1 Characteristics of distinct groups via T-N mismatch clustering for 184 A+ symptomatic patients

Group (n)	Description	Age	Sex (F/M)	Diagnosis (MCI/Dem)	Educ (SD)	MMSE (SD)	CDRSB (SD)	IT Tau SUVR (SD)
Group1 (96)	Canonical	76.5 (7.2)	45/51	60/36	15.4 (2.5)	25.8 (3.4)	2.85 (2.0)	1.46 (0.40)
Group2 (31)	Limbic vulnerable	79.9 (6.6)	12/19	9/22*	16.5 (2.5)	22.8*** (4.3)	5.94*** (4.1)	1.49 (0.40)
Group3 (12)	Diffuse vulnerable	81.0 (10)	2/10	4/8	15.2 (3.3)	23.8 (5.3)	4.27 (3.2)	1.41 (0.45)
Group4 (21)	Posterior-temporal occipital resilient	70.4* (7.1)	13/8	16/5	15.7 (2.7)	26.3 (3.6)	3.88 (3.6)	1.55 (0.38)
Group5 (19)	Anterior-temporal resilient	72.3 (8.5)	7/12	17/2	17.5* (2.4)	27.2 (2.7)	1.38 (1.3)	1.40 (0.32)
Group6 (5)	Mixed	73.7 (6.6)	2/3	2/3	15.0 (3.0)	25.0 (4.6)	2.10 (1.7)	1.66 (0.31)
Group Diff.	-	$p < 0.001$	$p = 0.191$	$p < 0.001$	$p = 0.024$	$p < 0.001$	$p < 0.001$	$p = 0.362$

Note: Overall group effects (p -values indicated in the bottom row) were tested using the Kruskal–Wallis test for categorical variables (sex, MCI/dementia) and linear regression for continuous variables (age, years of education, Mini-Mental State Examination [MMSE], Clinical Dementia Rating Sum of boxes [CDRSB], and inferior temporal (IT) tau SUVR). The baseline cognitive scores (MMSE⁴³, CDRSB³⁹) and IT Tau SUVR were compared with age, sex, and years of education as covariates. The mean (SD) is shown for age, years of education, MMSE, CDRSB, and IT tau SUVR. Pairwise comparisons of these variables between T-N groups were obtained. Only significant pairwise comparisons between T-N groups the Group1 (canonical) were marked in the table alongside the corresponding value. The p -values were adjusted by Bonferroni multiple comparison correction ($*p < 0.05$, $***p < 0.001$).

brain age gap was calculated by the difference between predicted brain age and the actual chronological age.

2.6 | Statistical analysis

Statistical analyses were performed in R (v4.5) or SPSS (v28). The between group comparison of continuous variables (e.g., regional tau SUVR) were analyzed by linear regression with covariates age and gender. Bonferroni correction was applied on all between-group comparisons. Comparison of ordinal or semi-quantitative variables (e.g., histology-measured TDP-43 severity levels) was conducted using Kruskal–Wallis tests³⁷ or using Mann-Whitney test³⁸ if only comparing between two groups. Additionally, a post-hoc analysis of the proportion of cases with the presence of any TDP-43 pathology was compared between autopsy groups using likelihood ratio chi-square test. The voxel-wise thickness comparison was analyzed by using the threshold-free cluster enhancement method³⁹ with age and gender as covariates. The global measure of Clinical Dementia Rating Sum of boxes (CDRSB)⁴⁰ were used to evaluate longitudinal cognitive changes. Longitudinal trajectories of cognitive scores were assessed with linear mixed-effects models⁴¹ using cognitive scores as the dependent variable. Fixed effects include time, group, and time*group interaction as predictors, and covariates (age, gender, and years of education). A random intercept was included in the mixed-effects model to account for correlations among repeated measures of cognitive scores. The follow up time ranged from 1 to 4 years and maximum of 4 time points for each participant. Significant differences in rate of change between groups was determined by comparing the slope of time*group interaction. All statistical tests were two-sided.

3 | RESULTS

3.1 | T-N groups were distinct despite similar AD severity

Based on T-N residuals, we clustered 184 A+ symptomatic (MCI/dementia) participants from the ADNI using hierarchical clustering³³ into six groups. The clinical characteristics of T-N groups are described in Table 1. These groups differed in age, proportion with MCI versus AD dementia diagnosis, years of education and degree of cognitive impairment. The groups did not differ in inferior temporal (IT) mean ¹⁸F-flortaucipir uptake ($p = 0.362$), a surrogate for AD severity^{42,43}; thus they do not appear to be simply reflective of AD severity per se. Average maps of T-N linear regression residuals across brain ROIs are represented visually for the six groups in Figure 2. The group with the largest number of participants ($n = 96$) displayed low overall residuals; as such, we labeled this group “canonical”. Two groups with greater neurodegeneration than expected given their level of tau ($N > T$, negative residuals) were labeled “vulnerable.” One of these groups had $N > T$ mostly in temporal/limbic regions, which we labeled as “limbic vulnerable” ($n = 31$); the other group ($n = 12$) displayed widespread $N > T$ throughout the cortex was labeled “diffuse vulnerable”. In addition, there were two T-N groups with less neurodegeneration than expected given the level of tau ($N < T$, positive residuals), and we labeled them as “resilient.” One ($n = 21$) displayed $N < T$ in posterior temporal to occipital cortex and was denoted as posterior-temporal occipital (PTO) resilient. We labeled the other group ($n = 19$) showing distinct $N < T$ in lateral and medial temporal cortex and parts of prefrontal cortex as anterior-temporal (AT) resilient. A final small group ($n = 5$) with $N < T$ especially along the motor cortex, but $N > T$ in temporal/limbic region, was labeled “mixed.”

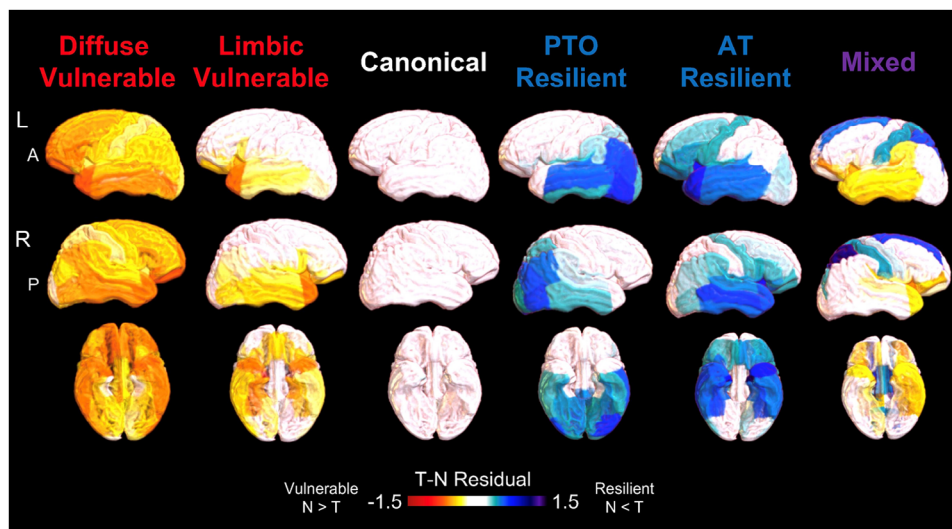


FIGURE 2 Average ROI-wise residual maps representing spatial T-N relationships for identified T-N groups among A+ symptomatic patients from ADNI via T-N mismatch: canonical (close to 0 residuals, $N \sim T$), vulnerable (negative residuals, $N > T$), resilient (positive residuals, $N < T$).

To determine in a more granular manner whether the T-N groups differed in tau burden, we assessed regional tau SUVR in representative limbic and cortical regions. Figure S2 further demonstrates that the groups did not differ in ^{18}F -flortaucipir uptake across limbic/cortical regions (P 's > 0.05). However, the between-group thickness covaried with regional tau, age, and sex differed in the same representative regions, supporting the contention of their “mismatch” status (Figure S2).

3.2 | Clustering A– symptomatic patients based on patterns of neurodegeneration alone reveals groups similar to those from T-N mismatch

Data-driven clustering of 159 MCI/dementia ADNI participants who were A– using regional control-referenced z-scores of cortical thickness was performed and referred to as “ N_z clustering”. We determined five N_z groups. Notably, the N_z group patterns of average z-score thickness resembled the residual patterns of the vulnerable T-N groups (Figure 1A). In particular, we found a group ($n = 11$) that had more negative z-scores in limbic regions, a pattern that resembled the T-N limbic vulnerable group, and we therefore labeled it as “limbic atrophy”. Two of the groups displayed relatively diffuse low z-scores that corresponded to the T-N diffuse vulnerable group and were combined (“diffuse atrophy”, $n = 26$; see Figure 1A) for additional analyses given their similar patterns (see Figure S3 for display of thickness map for these two groups separately). The largest group ($n = 114$) displayed minimal evidence of atrophy based on the control-referenced z-scores, which we labeled it as “no-atrophy”. Finally, a small group ($n = 8$) with more positive z-scores of cortical thickness in posterior temporal and occipital regions had a very similar pattern to the residual map of the T-N PTO resilient group, and was labeled as “PTO increased thickness”.

To assess the correspondence between these N_z groups with their mapped T-N mismatch group, we measured Euclidean distance as described in Methods and observed that this distance was lowest for the A– N_z groups to the T-N groups that we visually designated as corresponding (Table S3). Moreover, the obtained Pearson correlation between averaged regional thickness Z-score in N_z groups and averaged T-N residuals in corresponding T-N groups as described in the Methods section was 0.870 ($p < 0.001$). We then assessed the robustness of the mapping between corresponding pairs of T-N and N_z groups by recomputing the correlation for all possible pairwise mappings between T-N and N_z groups, which resulted in a distribution of much weaker correlation coefficients of 0.029 (± 0.40), suggesting a high degree of overlapping spatial patterns in corresponding groups as obtained through qualitative matching. Overall, the overlap between spatial patterns of residuals in the T-N mismatch groups in A+ and those of cortical thickness in the corresponding N_z groups in A– (Figure 1A) is consistent with the notion that T-N residuals reflect non-AD related phenomenology which may be present irrespective of amyloid status.

It is not surprising that the N_z group had less representation of “resilient” groups, as in symptomatic individuals without AD, there is no defined dominant neuropathology against which resilience can be measured. Aligning with the T-N groups, N_z groups also varied in clinical characteristics in a similar fashion. For example, the PTO increased thickness group was younger than the no-atrophy group, and the limbic atrophy group showed poorer baseline cognition (Table S4). The N_z groups did not differ in inferior temporal mean ^{18}F -flortaucipir uptake values, which were generally at a level below a typical threshold for “positive” T.⁴³

Next, we performed voxel-wise comparison of cortical thickness of each group from both the T-N and N_z clustering results with 137 A– cognitively normal participants from ADNI. We predicted that patterns of cortical thinning would reflect, to a large extent, regional

aspects of T-N mismatch patterns overlaid on typical AD effects in the T-N groups. Figure 1B shows voxels with significant differences in thickness ($P_{FWER} < 0.05$), controlling for age and sex, from cognitively normal individuals for both T-N and N_Z groups. As expected, the T-N canonical group displayed atrophy in the medial temporal lobe and posterior neocortical regions, corresponding to a “typical” pattern of AD pathology. Also expected, given how it was derived, the N_Z no-atrophy group did not differ from normal controls in cortical thickness. Alternatively, cortical thinning relative to controls was strikingly similar between T-N vulnerable and N_Z atrophy groups, although somewhat more extensive in the former likely stemming from the concomitant presence of AD-related neurodegeneration. The T-N limbic vulnerable and N_Z limbic atrophy groups both displayed prominent atrophy in temporal/limbic regions, while the T-N diffuse vulnerable and N_Z diffuse atrophy groups displayed more widespread atrophy throughout the temporal, parietal/occipital and frontal lobes. The T-N mixed group was excluded for voxel-wise comparison due to its small size. The T-N resilient groups and N_Z PTO increased thickness group did not display thickness differences with cognitively normal controls. As age is a resilience/vulnerability factor, the fact that PTO resilient group was the youngest group (Table S4) may account for differences in the regional N_Z patterns (Figure 1A) and the voxel-wise analysis, the latter of which was controlled by age and gender (Figure 1B), as well as having a stricter threshold of significance.

We also directly compared cortical thickness between groups with the respective canonical or no-atrophy groups in both T-N and A- N_Z groups respectively (Figure S4). T-N vulnerable and N_Z atrophy groups displayed significant reduction in cortical thickness relative to the respective T-N canonical or N_Z no-atrophy groups whereas the T-N resilient and N_Z PTO increased thickness groups displayed regions of increased cortical thickness. No significant voxel-wise differences were observed for any of these groups in the opposite direction (vulnerable/atrophy > canonical/no atrophy, resilient/increased thickness < canonical/no-atrophy).

3.3 | T-N groups were modulated by specific non-AD factors

We sought to explore factors that may influence the degree of neurodegeneration beyond AD and, thus, may drive patterns seen in the resilient versus vulnerable groups. We compared these possible modulators in both T-N groups and N_Z groups, reasoning that if these groups represent the presence of concomitant non-AD pathologies, they should show a similar association with measures suggestive of these pathologies (e.g., WMH associated with cerebrovascular disease).

In our prior work,²⁰ we demonstrated that relative mismatch of T and N was linked to age, as age is associated with atrophy in the absence of AD pathology. However, brain aging varies across individuals, and there are some that exhibit accelerated brain age changes for their chronological age and those that have younger appearing brains.^{44,45} We reasoned that accelerated or decelerated brain age

may be a source of vulnerability or resilience beyond chronological age and would have a similar influence on T-N and N_Z groups.

To assess this, we calculated “brain age gap,” which is the difference between the MRI-based brain age prediction and chronological age. Figure 1C plots the “brain age gap” for the T-N and N_Z groups. The limbic vulnerable T-N group was associated with significantly greater brain age gap (brain age > chronological age) than the canonical group ($p < 0.001$), but this effect was not significant for the diffuse vulnerable group. Brain age gap in both N_Z atrophy groups similarly demonstrated a significantly greater brain age gap compared to the no-atrophy group ($p < 0.001$). The similarity of these effects between the T-N and N_Z groups supports the idea that accelerated or decelerated brain aging is a factor that drives T-N mismatch which could also be present in non-AD symptomatic cases.

Another potential modulator of N outside of T is the presence of cerebrovascular disease. To further study this, we assessed the volume of WMH, a surrogate for cerebrovascular disease⁴⁶ with age included as a covariate (Figure 1D), as well as number of vascular risk factors⁴⁶ (Figure 1E). We found that the T-N vulnerable groups had significantly higher WMH volume compared to the T-N canonical group, which was consistent with prior our work.²⁰ The diffuse vulnerable group had a very strong effect ($p < 0.001$) and was also associated with greater number of vascular risk factors ($p < 0.01$) than the canonical group (Figure 1D, E). Likewise, among N_Z groups, the diffuse atrophy group displayed significantly higher WMH ($p < 0.001$) and greater number of vascular risk factors ($p < 0.01$) compared to the no-atrophy group.

3.4 | Post mortem T-N groups were associated with co-pathologies

We next attempted to determine a potential link between histological evidence of concomitant proteinopathies, TDP-43 and alpha-synuclein, with T-N mismatch groups. In particular, we hypothesized that the T-N limbic vulnerable group would display evidence of concomitant TDP-43 pathology, such as that observed in limbic-predominant age-related TDP-43 encephalopathy (LATE),⁴⁷ given the link between LATE and greater medial temporal lobe (MTL) involvement in AD.⁴⁸ We used 98 A+ autopsies from the Brain Bank of the University of Pennsylvania Center for Neurodegenerative Disease Research (CNDP) and *ante mortem* MRI. We obtained five groups through the same clustering approach as for the in vivo data and compared thickness across the entire brain to the canonical group (Figure 3A). We observed similar patterns of thickness differences to what were described in the preceding in vivo analyses (Figure S4). We therefore denoted these groups as limbic vulnerable, diffuse vulnerable, PTO resilient and AT resilient, in addition to a canonical group. Demographics are presented in Table S5.

We analyzed TDP-43 pathology in regions associated with early stages of LATE neuropathic change (LATE-NC) across the different T-N mismatch groups (Figure 3B). Consistent with our hypothesis, we found the limbic vulnerable group was the only group with significantly higher TDP-43 severity than the canonical group in the medial

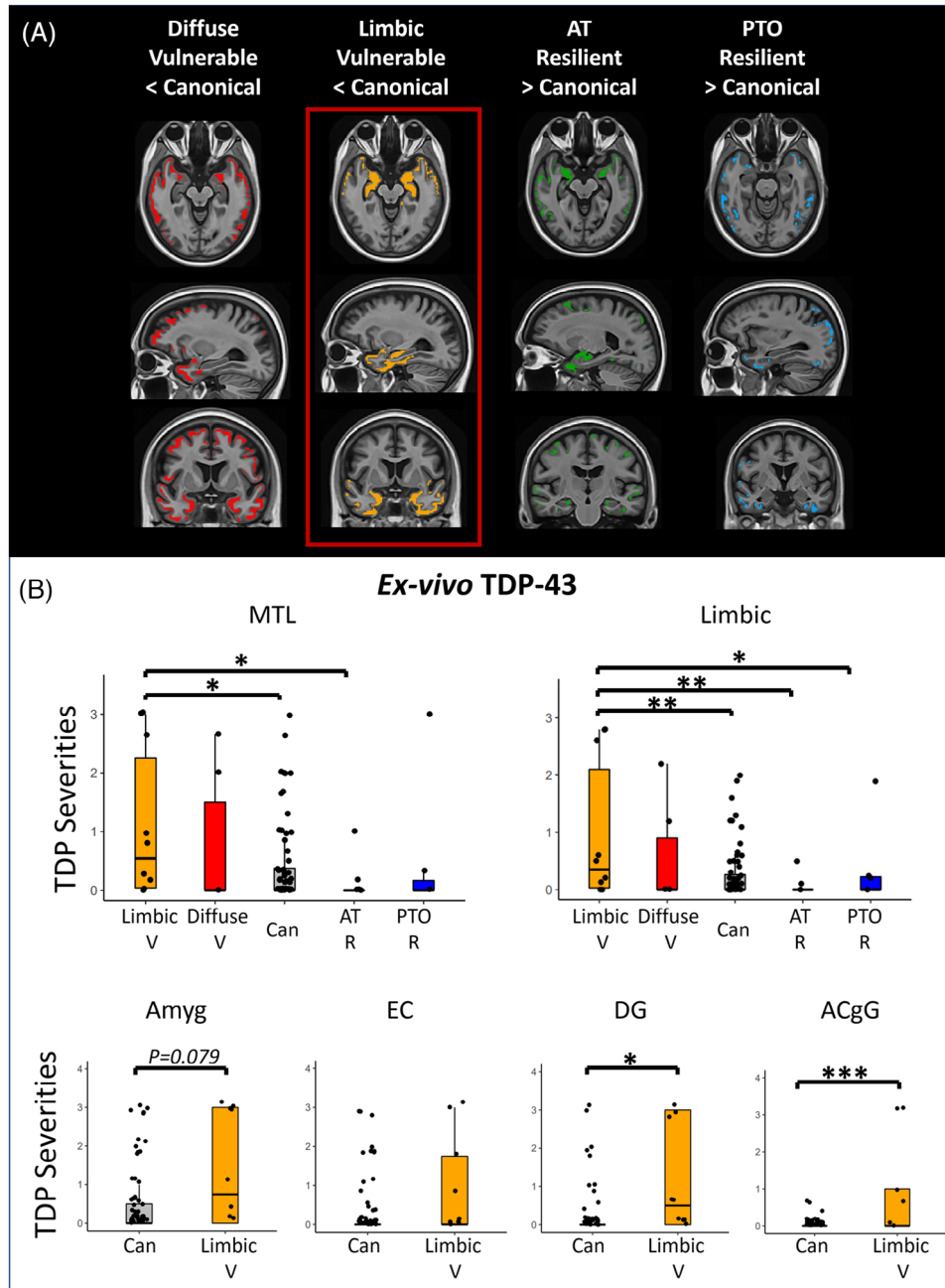


FIGURE 3 Post mortem assessment of TDP-43 on T-N groups of CNDR autopsies with CERAD score ≥ 2 (A) Voxel-wise significant differences of *ante mortem* thickness between vulnerable/resilient groups and the canonical group with $P_{FWER} < 0.05$ for CNDR autopsies. The colored areas represent significant difference with the canonical for each group. (B) The between-group comparison of *ex-vivo* TDP-43 burden of CNDR cohort in medial temporal lobe, a limbic composite ROI as well as semi-quantitative TDP-43 severities across representative regions of early TDP-43 deposition including amygdala (Amyg), entorhinal cortex (EC), dentate gyrus (DG), and anterior cingulate gyrus (ACgG). The comparisons were not corrected by multiple comparisons given that we specifically predicted that the limbic vulnerable group would be associated with TDP-43 pathology in this case rather than performing exploratory analysis. Significant levels are denoted as * $p < 0.05$, ** $p < 0.01$, *** $p < 0.001$.

temporal lobe region (MTL, $p = 0.023$) as well as in a composite limbic region ($p < 0.01$). Moreover, the limbic vulnerable group was associated with higher TDP-43 burden in regions of early TDP-43 deposition including amygdala (Amyg, $p = 0.079$), entorhinal cortex (EC, $p = 0.179$), dentate gyrus (DG, $p = 0.014$), and anterior cingulate gyrus (ACgG, $p < 0.001$) compared to the canonical group (Figure 3B). Note that these differences did not survive correction for multiple

comparisons, but were consistent with a strong a priori hypothesis. Interestingly, the AT resilient group displayed the least amount of TDP-43 in MTL and limbic regions which was significantly lower than limbic vulnerable group ($p < 0.05$), but was not significant in comparison to the canonical group ($p > 0.05$). As a post-hoc analysis, we also compared the proportion of cases in the limbic vulnerable group having any kind of TDP-43 pathology with those in the canonical

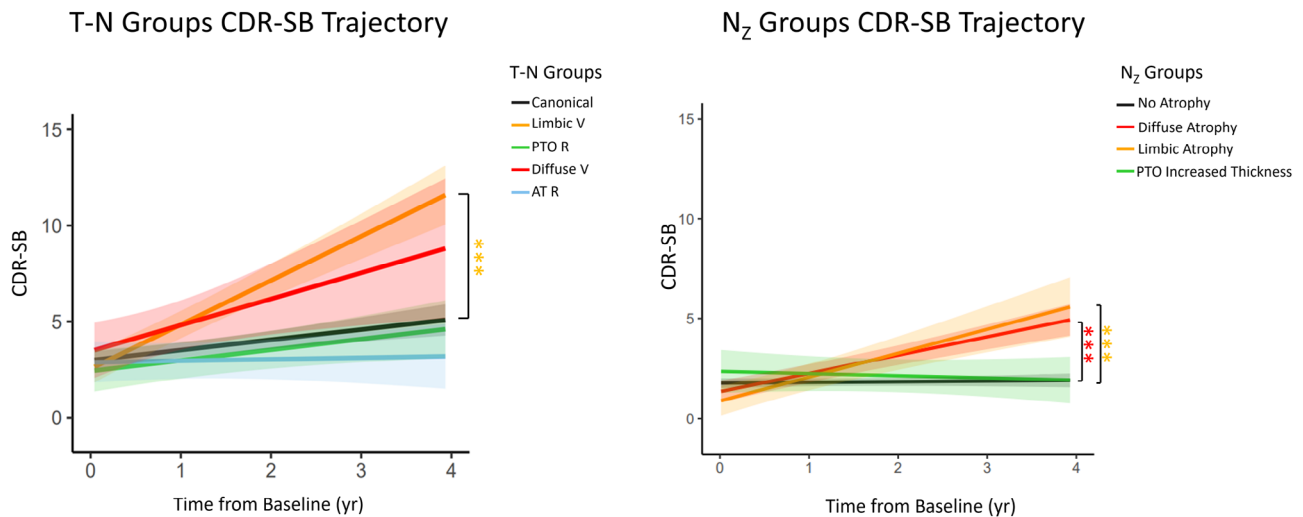


FIGURE 4 Longitudinal CDR-SB changes for all T-N groups (left) and N₂ groups (right) of ADNI cohort covaried with age, sex, years of education and baseline CDR-SB score. The shadow represents 95% confidence intervals. The mixed group was excluded in the analysis of T-N group comparison due to small sample size. Only significant comparisons with the typical group (canonical for T-N groups, no atrophy group for N₂ groups) were marked. Significant levels after Bonferroni multiple comparison correction are denoted as *** $p < 0.001$.

group and found that the difference was significant (70% in limbic vulnerable group versus 34% in canonical group, $p < 0.05$). As not all cases had intermediate or high ADNC ($n = 11$), we repeated the analysis including only such cases (Table S6). The results were highly similar with regard to relationship of groups with TDP-43 (Figure S5).

We also examined alpha-synuclein levels between groups specifically in amygdala, MTL, and limbic composite region given early involvement in those structures. We did not find group differences ($p = 0.86$ for Amyg, $p = 0.33$ for MTL, $p = 0.36$ for limbic composite ROI). Similar to in vivo T-N groups, the *post mortem* T-N groups also differed in cognition with the limbic vulnerable group showed significantly worse MMSE than the canonical group (Table S5).

3.5 | T-N mismatch predicts longitudinal cognitive changes

In light of the potential role for the presence or absence of co-pathologies on longitudinal trajectory of decline, we examined differences in CDR-SB change, a measure that incorporates cognitive and functional data, among the different T-N mismatch groups from ADNI. We predicted that T-N vulnerable groups would display faster cognitive decline over time due to the possibility of comorbid pathologies while resilient groups would be expected to have slower decline. Figure 4 Left displays longitudinal CDR-SB performance for different T-N groups. The T-N limbic vulnerable group displayed significantly steeper CDR-SB increases than canonical ($p < 0.001$). The diffuse vulnerable tended to progress faster, but this difference did not reach statistical significance. Alternatively, the AT resilient group tended to progress slower although not significantly so relative to the canonical group after multiple comparisons correction.

We also examined longitudinal cognitive changes in the N₂ groups (Figure 4 Right). We predicted similar relative decline between analogous groups to the T-N analysis, but slower rates of decline due to absence of concomitant AD. Indeed, the N₂ atrophy groups displayed a faster rate of decline than the no atrophy group ($p < 0.001$ for limbic atrophy, $p < 0.001$ for diffuse atrophy), consistent with the expectation that non-AD pathologies would be driving decline. Moreover, the average annualized rate of change for T-N limbic vulnerable (2.23 points/year) and T-N diffuse vulnerable (1.32 points/year) groups were both greater than the rates for N₂ limbic atrophy (1.17 points/year) and diffuse atrophy (0.92 points/year) groups.

3.6 | Application of T-N mismatch to individual patients

To assess the transferability of T-N mismatch and its potential clinical utility on classification of individuals, we applied the T-N mismatch framework to an independent testing cohort, referred to as "AVID", using existing T-N residual models and then inferred their T-N group identity. The testing cohort contained 71 symptomatic A+ patients, including 29 with dementia and 42 with MCI. The regional T-N residuals of each patient was obtained by projecting their T-N relationship on the existing regional T-N regressions models in the ADNI cohort. Group assignment for each individual patient was then identified by finding the ADNI T-N group with the *lowest distance* based on these imputed residuals (see the Methods section for details). We then grouped the patients based on inferred T-N group identity and visualized their average T-N residual maps (Figure S6). The averaged Euclidean distance of individuals from classified T-N groups in AVID cohort to prior T-N groups in ADNI is provided (Table S7), in which the AVID T-N groups showed the closest Euclidean distance to the corresponding ADNI

T-N groups. To investigate the likelihood that a random spatial pattern of residuals would yield a closer distance metric than the actual data in the “forced choice” paradigm, we conducted a bootstrapping experiment that randomly permuted thickness values for each region between patients while keeping the regional tau the same over 1000 iterations. In each bootstrapping experiment, each patient's Euclidean distance to the closest prior six T-N groups were obtained and averaged across all patients. The averaged Euclidean distance using the same forced choice approach was 3.99 with standard deviation as 0.02 from 1000 times bootstrapping. The probability of reaching the original averaged distance for the study in the manuscript which was 3.17 or lower was $p < 0.001$. We also computed Pearson correlation between averaged T-N residuals of ADNI T-N groups and those in classified AVID groups, and obtained 0.80 as correlation coefficient ($p < 0.0001$). The distribution of correlation coefficients when using all possible non-matching, pairwise mappings of T-N and classified AVID groups was much weaker (0.041 ± 0.3), again suggesting a high degree of overlapping spatial patterns in corresponding groups. Likewise, they were associated with clinical differences similar to that of ADNI (Table S8), including the limbic vulnerable group displaying the poorest MMSE and Alzheimer's disease assessment scale cognitive subscale-11 (ADAS-Cog11) scores among all groups and the resilient groups generally performing better than the other groups.

4 | DISCUSSION

Prior work²⁰ from our group introduced a data-driven framework to study variability in T-N relationship in cognitively impaired individuals on the AD continuum that could help characterize the potential role of non-AD pathologies. Here, we first replicate previous findings²⁰ in a larger dataset. We then present multiple validation experiments to explore the power of this framework and its potential clinical utility.

In a cohort of cognitively impaired A+ individuals, we identified six data-driven groups associated with different spatial patterns of T-N relationships. The largest group was defined as “canonical”, in which the T-N relationship was close to the regression line in all regions (i.e., $N \sim T$). A limbic vulnerable group displayed greater neurodegeneration than tau ($N > T$) in limbic regions, while a diffuse vulnerable group displayed $N > T$ throughout the cortex. Conversely, there were groups with relatively less neurodegeneration given tau ($N < T$) that we classified as PTO resilient or anterior-temporal resilient based on the spatial pattern. These results replicated, in a larger cohort, those reported in Das et al.²⁰

In this work, we then test the hypothesis that the T-N mismatch groups in A+ are driven by non-AD factors. We predicted that in individuals with non-AD etiologies to their cognitive impairment (A– symptomatic individuals), we would observe patterns of cortical thinning analogous to the T-N mismatch residuals where AD-related effects are *conceptually* removed. Indeed, many of the residual patterns of the T-N groups in the A+ cohort also appeared in A– symptomatic individuals. Similarities between these A– N_z groups and the T-N groups support the hypothesis that the T-N residuals reflect the non-

AD factors that contribute to neurodegeneration concomitant with AD pathology.

One such important non-AD factor is age. Age, independent of AD pathology, is associated with structural changes that may dissociate to varying degrees with AD-related neurodegeneration.^{7,49} However, *brain age* also varies across individuals, with some exhibiting more accelerated brain age for their chronological age and vice versa. Decelerated versus accelerated brain aging may be a potential source of brain resilience and vulnerability in the context of AD and other neurodegenerative conditions. To test this hypothesis, we examined a measure of brain age gap in the T-N groups that was specifically designed using a machine learning approach to dissociate age-related brain changes from that of AD (SPARE-BA), such that it was most dependent on patterns of atrophy in regions less affected by AD (e.g., subcortical gray matter and cerebellum).⁷ Indeed, the vulnerable groups tended to have older brain age relative to chronological age (accelerated aging) compared to the canonical group. This suggests that variability in brain aging, beyond chronological age, may also influence vulnerability to AD pathology. However, one caution is that this measure was not designed to account for non-AD pathologies which also may modulate its prediction.

Indeed, non-AD co-pathologies are very common in individuals with AD pathology and are likely important contributors to the heterogeneity of AD.^{1–3,5,6} The “limbic vulnerable” group showed greater neurodegeneration relative to tau pathology in temporal lobe, including temporal pole, and orbital frontal cortex. This group also displayed generally greater cortical thinning in these regions when directly compared to the canonical group, controlling for age and sex, despite similar inferior temporal tau burden. While there may be other colocalized non-AD pathologies (e.g., argyrophilic grain disease), a particularly important pathology associated with limbic involvement is TDP-43, especially LATE,⁴⁷ a common co-pathology with AD. LATE can accelerate cognitive progression and hippocampal atrophy when co-occurring with AD relative to AD alone,^{6,50} although it can also occur independently.⁴⁷ The pattern observed in this group is consistent with expected regional distribution of pathology and atrophy observed in LATE.^{47,51,52} This group demonstrated a more rapid rate of cognitive decline relative to the canonical group, also consistent with prior work^{47,50,53} studying this co-pathology in the setting of AD. Moreover, this group was recapitulated in the *post mortem* analysis demonstrating an atrophy pattern remarkably similar to that in the *in vivo* group. Most importantly, this T-N group demonstrated higher levels of TDP-43 deposition in MTL and limbic regions compared to other T-N groups, including the canonical group, supporting the hypothesis that TDP-43 proteinopathy drives limbic T-N mismatch.

In contrast, the T-N resilient groups, especially the AT resilient group with $N < T$ predominantly in temporal regions, tended to contain the least amount of TDP-43 in MTL based on the *post mortem* analysis. Individuals in this group may be particularly resistant to TDP-43 pathology. It has been argued that resilience to AD may partly depend on resistance to TDP-43, or other pathologies.⁵⁴ Given that even the canonical group in the *post mortem* analysis had some degree of TDP-43 pathology and that comorbidity is extremely common in AD

(Figure 3B), perhaps the canonical group is actually a mixed pathology group, and it is the “resilient” groups that lack co-pathology. The canonical group, rather than being “pure” AD, thus, may contain a medium level of co-pathologies; the AT resilient and limbic vulnerable groups then may be associated with the least and the most TDP-43 severities, respectively.

Another factor that is thought to provide some resilience to pathology is education.⁵⁵ Indeed, the AT resilience T-N group had significantly greater years of education (Table 1). Nevertheless, the significance of this association was mild. Replication in other samples will be needed to study if the effect is consistent. Moreover, gender could be a potential modulating factor for T-N mismatch. Although we did not find any significant difference in gender between T-N groups, the *in vivo* PTO resilient group tended to have more female participants. There is relatively consistent data in the literature⁵⁶ that tau levels are higher in females, which may reflect their ability to mask more disease due to resilience. Future work can further explore the role of gender in resilience.

The diffuse vulnerable group had greater WMH volume and number of vascular risk factors⁵⁷ compared to the canonical group, controlling for age, suggesting that cerebrovascular pathology may contribute to the apparent “vulnerability” in this group. Alternatively, the AT resilient group tended to have lower WMH volumes than the canonical group, but did not reach statistical significance. This group also displayed less thinning in temporal regions. There are some data^{3,58} suggesting that TDP-43 is more common in the setting of cerebrovascular factors such that its absence may allow for AT resilience to TDP-43. Further, aligning with TDP-43 findings above, the canonical group had evidence of an intermediate degree of vascular disease between AT resilient and diffuse vulnerable, akin to a continuum of cerebrovascular pathology (AT resilient < canonical < diffuse vulnerable). This again suggests that the degree of co-pathology may modulate relative resilience or vulnerability, but that “typical” AD is marked by modest degree of other pathologies, consistent with autopsy data.

Clustering based on A– thickness also produced a more diffuse atrophy group with high levels of WMHs and vascular risk factors while those with less atrophy had less evidence of small vessel disease. The replication of these patterns in the N_z groups again supports the hypothesis that T-N mismatch is teasing out non-AD modulators of resilience and vulnerability.

Importantly, we found that T-N *mismatch* groups differed not only in cross-sectional, but also longitudinal cognitive outcomes, consistent with our prior work in a smaller cohort.²⁰ Vulnerable groups declined faster than the canonical groups, likely attributable to the presence of non-AD pathologies. In the setting of AD, tau and other pathologies may synergistically interact to accelerate cognitive impairment.^{6,50,53} These findings are consistent with other work demonstrating that comorbid pathologies contribute to dementia phenotype and course.^{6,59,60} Moreover, the AT resilient group demonstrated relatively little evidence of progression although not statistically different from the modest longitudinal decline in the canonical group. Thus, T-N mismatch may have implications for prognosis and potential stratification in intervention studies. Interestingly, the paral-

lel N_z groups displayed qualitatively similar, but generally less steep CDR-SB decline, consistent with the expectation that AD plus other comorbidities result in faster decline than non-AD drivers of decline alone.^{6,50,53,59}

As further support for the robustness and potential clinical utility of the T-N mismatch framework, we made portable and straightforward inference of T-N group for individual patients in an independent cohort, based on an existing T-N residual model. Inferred phenotypic groups shared clinical characteristics with the training cohort. This indicates that T-N mismatch modeling may be generalizable and therefore may have clinical utility and holds promise for personalized medicine. These T-N groups were also largely reproducible in the *post mortem* cohort. Finally, similar, although not completely, overlapping phenotypes were also found using an alternative marker of neurodegeneration, ¹⁸F-fluorodeoxyglucose PET, in our prior work.²¹

Our study has some limitations. First, while we used linear regression to establish T-N mismatch, T-N relationship is likely, to some extent, non-linear even in pure AD cases. Non-linear approaches, including image-to-image translation, may better model T-N relationships, including possible remote spatial dependence between network hubs and connected nodes. Second, some degree of arbitrariness in decisions around the number of clusters limits the robustness of the data driven clustering framework. Extracting clusters at different resolution levels could potentially provide insights about broader or finer parcellation of phenotypes. Third, our *ex vivo* analysis utilized only six ROIs due to specimen availability and semi-quantitative measures of tau pathology, which further limits the sensitivity for assessment of deviations. Nonetheless, groups from this *post mortem* dataset were similar to those in our *in vivo* analysis. Another limitation to histology is that PHF-1 is not specific to tau neurofibrillary tangles, potentially conflating other non-AD tauopathy contributions. Last, the dataset sizes were relatively modest. Therefore, the results may not generalize to other cohorts with greater numbers of co-morbidities and race/ethnicities that are not well represented in ADNI.

In summary, our findings demonstrate that T-N *mismatch* depicts vulnerability and resilience likely attributable to specific non-AD pathologies or resilience factors. This approach may therefore provide important characterization of phenotypic heterogeneity in clinical populations, with implications for therapeutic trials and management.

ACKNOWLEDGMENTS

We acknowledge posthumously the significant contribution of John Q. Trojanowski and Murray Grossman to this work and the field of Alzheimer's disease. We acknowledge the brain donors in CNDR and their families. The study was supported by the funding R01 AG056014 and RF1 AG069474. The CNDR brain bank was funded by NIH (P01AG066597, P30AG072979, U19AG062418). This study was also supported by MultiPark—A Strategic Research Area at Lund University. The AVID cohort in this work was sponsored by Avid Radiopharmaceuticals. Data collection and sharing for this project was

funded by the Alzheimer's Disease Neuroimaging Initiative (ADNI) (National Institutes of Health Grant U01 AG024904) and DOD ADNI (Department of Defense award number W81XWH-12-2-0012). ADNI is funded by the National Institute on Aging, the National Institute of Biomedical Imaging and Bioengineering, and through generous contributions from the following: AbbVie, Alzheimer's Association; Alzheimer's Drug Discovery Foundation; Araclon Biotech; BioClinica, Inc.; Biogen; Bristol-Myers Squibb Company; CereSpir, Inc.; Cogstate; Eisai Inc.; Elan Pharmaceuticals, Inc.; Eli Lilly and Company; EuroImmun; F.Hoffmann-La Roche Ltd and its affiliated company Genentech, Inc.; Fujirebio; GE Healthcare; IXICO Ltd.; Janssen Alzheimer Immunotherapy Research & Development, LLC.; Johnson & Johnson Pharmaceutical Research & Development LLC.; Lumosity; Lundbeck; Merck & Co., Inc.; Meso Scale Diagnostics, LLC.; NeuroRx Research; Neurotrack Technologies; Novartis Pharmaceuticals Corporation; Pfizer Inc.; Piramal Imaging; Servier; Takeda Pharmaceutical Company; and Transition Therapeutics. The Canadian Institutes of Health Research is providing funds to support ADNI clinical sites in Canada. Private sector contributions are facilitated by the Foundation for the National Institutes of Health (www.fnih.org). The grantee organization is the Northern California Institute for Research and Education, and the study is coordinated by the Alzheimer's Therapeutic Research Institute at the University of Southern California. ADNI data are disseminated by the Laboratory for Neuro Imaging at the University of Southern California.

CONFLICT OF INTEREST STATEMENT

D.A.W. has served as a paid consultant to Eli Lilly and Qynapse. He serves on a DSMB for Functional Neuromodulation. He is a site investigator for a clinical trial sponsored by Biogen. I.M.N serves as speakers bureau for Biogen and advisory board for Eisai. L.X. received personal consulting fees from Galileo CDS, Inc. He has become an employee of Siemens Healthineers since May 2022 but the current study was conducted during his employment at the University of Pennsylvania. C.T.M. receives an honorarium as Associate Editor of *Neuroimage: Clinical*. B.C.D. has received consulting fees from Acadia, Alector, Arkuda, Biogen, Denali, Eisai, Genentech, Lilly, Merck, Takeda, Wave LifeSciences. S.R.D. has received consulting fees from Rancho Biosciences and NIA Therapeutics. All other authors declare no conflicts of interest. Author disclosures are available in the [supporting information](#).

CONSENT STATEMENT

We confirm that all human subjects provided informed consent. Human brain specimens were obtained in accordance with the State of Pennsylvania and University of Pennsylvania Institutional Review Board guidelines. Where possible, pre-consent during life and, in all cases, next-of-kin consent at death was given.

CLINICAL TRIAL

The clinical trial registration number for Alzheimer's Disease Neuroimaging Initiative 3 (ADNI3) Protocol (ADNI3) is NCT02854033. The clinical trial registration number for Avid (A05) is NCT02016560.

REFERENCES

- Kapasi A, DeCarli C, Schneider JA. Impact of multiple pathologies on the threshold for clinically overt dementia. *Acta Neuropathol (Berl)*. 2017;134(2):171-186. doi:10.1007/s00401-017-1717-7
- Kapasi A, Schneider JA. Vascular contributions to cognitive impairment, clinical Alzheimer's disease, and dementia in older persons. *Biochim Biophys Acta*. 2016;1862(5):878-886. doi:10.1016/j.bbadis.2015.12.023
- Katsumata Y, Fardo DW, Kukull WA, Nelson PT. Dichotomous scoring of TDP-43 proteinopathy from specific brain regions in 27 academic research centers: associations with Alzheimer's disease and cerebrovascular disease pathologies. *Acta Neuropathol Commun*. 2018;6(1):142. doi:10.1186/s40478-018-0641-y
- Cummings JL. Cognitive and behavioral heterogeneity in Alzheimer's disease: seeking the neurobiological basis. *Neurobiol Aging*. 2000;21(6):845-861. doi:10.1016/S0197-4580(00)00183-4
- Lamar M, Boots EA, Arfanakis K, Barnes LL, Schneider JA. Common brain structural alterations associated with cardiovascular disease risk factors and Alzheimer's dementia: future directions and implications. *Neuropsychol Rev*. 2020;30(4):546-557. doi:10.1007/s11065-020-09460-6
- Robinson JL, Richardson H, Xie SX, et al. The development and convergence of co-pathologies in Alzheimer's disease. *Brain*. 2021;144(3):953-962. doi:10.1093/brain/awaa438
- Hwang G, Abdulkadir A, Erus G, et al. Disentangling Alzheimer's disease neurodegeneration from typical brain ageing using machine learning. *Brain Commun*. 2022;4(3):fcac117. doi:10.1093/braincomms/fcac117
- Bartrés-Faz D, Arenaza-Urquijo E, Ewers M, et al. Theoretical frameworks and approaches used within the Reserve, Resilience and Protective Factors professional interest area of the Alzheimer's Association International Society to Advance Alzheimer's Research and Treatment. *Alzheimers Dement Amst Neth*. 2020;12(1):e12115. doi:10.1002/dad2.12115
- Stern Y, Arenaza-Urquijo EM, Bartrés-Faz D, et al. Whitepaper: defining and investigating cognitive reserve, brain reserve, and brain maintenance. *Alzheimers Dement*. 2020;16(9):1305-1311. doi:10.1016/j.jalz.2018.07.219
- Ossenkoppele R, Lyoo CH, Jester-Broms J, et al. Assessment of demographic, genetic, and imaging variables associated with brain resilience and cognitive resilience to pathological tau in patients with Alzheimer disease. *JAMA Neurol*. 2020;77(5):632. doi:10.1001/jamaneurol.2019.5154
- Lesuis SL, Hoeijmakers L, Korosi A, et al. Vulnerability and resilience to Alzheimer's disease: early life conditions modulate neuropathology and determine cognitive reserve. *Alzheimers Res Ther*. 2018;10(1):95. doi:10.1186/s13195-018-0422-7
- Whitwell JL, Josephs KA, Murray ME, et al. MRI correlates of neurofibrillary tangle pathology at autopsy: a voxel-based morphometry study. *Neurology*. 2008;71(10):743-749. doi:10.1212/01.wnl.0000324924.91351.7d
- Wisse LEM, Ravikumar S, Ittyerah R, et al. Downstream effects of pathology on neurodegeneration of medial temporal lobe subregions. *Acta Neuropathol Commun*. 2021;9(1):128. doi:10.1186/s40478-021-01225-3
- Ravikumar S, Wisse LEM, Lim S, et al. Ex vivo MRI atlas of the human medial temporal lobe: characterizing neurodegeneration due to tau pathology. *Acta Neuropathol Commun*. 2021;9(1):173. doi:10.1186/s40478-021-01275-7
- Joie RL, Visani AV, Baker SL, et al. Prospective longitudinal atrophy in Alzheimer's disease correlates with the intensity and topography of baseline tau-PET. *Sci Transl Med*. 2020;12(524). doi:10.1126/scitranslmed.aau5732

16. Harrison TM, Joie RL, Maass A, et al. Longitudinal tau accumulation and atrophy in aging and alzheimer disease. *Ann Neurol*. 2019;85(2):229-240. doi:10.1002/ana.25406
17. Joie RL, Visani A, Bourakova V, et al. [P2-373]: aV1451-PET CORTICAL UPTAKE AND REGIONAL DISTRIBUTION PREDICT LONGITUDINAL ATROPHY IN ALZHEIMER'S DISEASE. *Alzheimers Dement*. 2017;13(7S_Part_15):P769-P769. doi:10.1016/j.jalz.2017.06.1028
18. Das SR, Xie L, Wisse LEM, et al. Longitudinal and cross-sectional structural magnetic resonance imaging correlates of AV-1451 uptake. *Neurobiol Aging*. 2018;66:49-58. doi:10.1016/j.neurobiolaging.2018.01.024
19. Ossenkoppele R, Smith R, Ohlsson T, et al. Associations between tau, A β , and cortical thickness with cognition in Alzheimer disease. *Neurology*. 2019;92(6):e601-e612. doi:10.1212/WNL.0000000000006875
20. Das SR, Lyu X, Duong MT, et al. Tau-atrophy variability reveals phenotypic heterogeneity in Alzheimer's disease. *Ann Neurol*. 2021;90(5):751-762. doi:10.1002/ana.26233
21. Duong MT, Das SR, Lyu X, et al. Dissociation of tau pathology and neuronal hypometabolism within the ATN framework of Alzheimer's disease. *Nat Commun*. 2022;13(1):1495. doi:10.1038/s41467-022-28941-1
22. Devous MD, Fleisher AS, Pontecorvo MJ, et al. Relationships between cognition and neuropathological tau in Alzheimer's disease assessed by 18F Flortaucipir PET. *J Alzheimers Dis JAD*. 2021;80(3):1091-1104. doi:10.3233/JAD-200808
23. Mirra SS, Heyman A, McKeel D, et al. The consortium to establish a registry for Alzheimer's Disease (CERAD). Part II. Standardization of the neuropathologic assessment of Alzheimer's disease. *Neurology*. 1991;41(4):479-486. doi:10.1212/wnl.41.4.479
24. Montine TJ, Phelps CH, Beach TG, et al. National Institute on Aging - Alzheimer's Association guidelines for the neuropathologic assessment of Alzheimer's disease: a practical approach. *Acta Neuropathol (Berl)*. 2012;123(1):1-11. doi:10.1007/s00401-011-0910-3
25. Tustison NJ, Cook PA, Klein A, et al. Large-scale evaluation of ANTs and FreeSurfer cortical thickness measurements. *NeuroImage*. 2014;99:166-179. doi:10.1016/j.neuroimage.2014.05.044
26. Wang H, Suh JW, Das S, Pluta J, Altinay M, Yushkevich P. Regression-based label fusion for multi-atlas segmentation. *Conf Comput Vis Pattern Recognit Workshop IEEE Comput Soc Conf Comput Vis Pattern Recognit Workshop*. 2011:1113-1120. doi:10.1109/CVPR.2011.5995382. Published online.
27. Das SR, Avants BB, Grossman M, Gee JC. Registration based cortical thickness measurement. *NeuroImage*. 2009;45(3):867-879. doi:10.1016/j.neuroimage.2008.12.016
28. Avants BB, Epstein CL, Grossman M, Gee JC. Symmetric diffeomorphic image registration with cross-correlation: evaluating automated labeling of elderly and neurodegenerative brain. *Med Image Anal*. 2008;12(1):26-41. doi:10.1016/j.media.2007.06.004
29. Landau SM, Breault C, Joshi AD, et al. Amyloid- β imaging with Pittsburgh compound B and florbetapir: comparing radiotracers and quantification methods. *J Nucl Med Off Publ Soc Nucl Med*. 2013;54(1):70-77. doi:10.2967/jnumed.112.109009
30. Jenkinson M, Bannister P, Brady M, Smith S. Improved optimization for the robust and accurate linear registration and motion correction of brain images. *NeuroImage*. 2002;17(2):825-841. doi:10.1016/s1053-8119(02)91132-8
31. Kuijf HJ, Biesbroek JM, De Bresser J, et al. Standardized assessment of automatic segmentation of white matter hyperintensities and results of the WMH segmentation challenge. *IEEE Trans Med Imaging*. 2019;38(11):2556-2568. doi:10.1109/TMI.2019.2905770
32. Toledo JB, Van Deerlin VM, Lee EB, et al. A platform for discovery: the University of Pennsylvania Integrated Neurodegenerative Disease Biobank. *Alzheimers Dement J Alzheimers Assoc*. 2014;10(4):477-484.e1. doi:10.1016/j.jalz.2013.06.003
33. Ward JH. Hierarchical grouping to optimize an objective function. *J Am Stat Assoc*. 1963;58(301):236-244. doi:10.1080/01621459.1963.10500845
34. Thorndike RL. Who belongs in the family. *Psychometrika*. 1953:267-276. Published online.
35. Rorden C, Brett M. Stereotaxic display of brain lesions. *Behav Neurol*. 2000;12(4):191-200. doi:10.1155/2000/421719
36. Bozdogan H. Model selection and Akaike's Information Criterion (AIC): the general theory and its analytical extensions. *Psychometrika*. 1987;52(3):345-370. doi:10.1007/BF02294361
37. Kruskal WH, Wallis WA. Use of ranks in one-criterion variance analysis. *J Am Stat Assoc*. 1952;47(260):583-621. doi:10.2307/2280779
38. Mann HB, Whitney DR. On a test of whether one of two random variables is stochastically larger than the other. *Ann Math Stat*. 1947;18(1):50-60. doi:10.1214/aoms/1177730491
39. Smith SM, Nichols TE. Threshold-free cluster enhancement: addressing problems of smoothing, threshold dependence and localisation in cluster inference. *NeuroImage*. 2009;44(1):83-98. doi:10.1016/j.neuroimage.2008.03.061
40. O'Bryant SE, Waring SC, Cullum CM, et al. Staging dementia using clinical dementia rating scale sum of boxes scores. *Arch Neurol*. 2008;65(8):1091-1095. doi:10.1001/archneur.65.8.1091
41. nlme: Linear and nonlinear mixed effects models - ScienceOpen. Accessed February 17, 2022. <https://www.scienceopen.com/document?vid=f71afca1-5770-4ec9-8abc-9f2da9326579>
42. Jack CR, Wiste HJ, Therneau TM, et al. Associations of amyloid, tau, and neurodegeneration biomarker profiles with rates of memory decline among individuals without dementia. *JAMA*. 2019;321(23):2316-2325. doi:10.1001/jama.2019.7437
43. Maass A, Landau S, Baker SL, et al. Comparison of multiple tau-PET measures as biomarkers in aging and Alzheimer's disease. *NeuroImage*. 2017;157:448-463. doi:10.1016/j.neuroimage.2017.05.058
44. Cole JH, Marioni RE, Harris SE, Deary IJ. Brain age and other bodily "ages": implications for neuropsychiatry. *Mol Psychiatry*. 2019;24(2):266-281. doi:10.1038/s41380-018-0098-1
45. Elliott ML, Belsky DW, Knodt AR, et al. Brain-age in midlife is associated with accelerated biological aging and cognitive decline in a longitudinal birth cohort. *Mol Psychiatry*. 2021;26(8):3829-3838. doi:10.1038/s41380-019-0626-7
46. Moroni F, Ammirati E, Hainsworth AH, Camici PG. Association of white matter hyperintensities and cardiovascular disease. *Circ Cardiovasc Imaging*. 2020;13(8):e010460. doi:10.1161/CIRCIMAGING.120.010460
47. Nelson PT, Dickson DW, Trojanowski JQ, et al. Limbic-predominant age-related TDP-43 encephalopathy (LATE): consensus working group report. *Brain*. 2019;142(6):1503-1527. doi:10.1093/brain/awz099
48. de Flores R, Wisse LEM, Das SR, et al. Contribution of mixed pathology to medial temporal lobe atrophy in Alzheimer's disease. *Alzheimers Dement*. 2020;16(6):843-852. doi:10.1002/alz.12079
49. Bakkour A, Morris JC, Wolk DA, Dickerson BC. The effects of aging and Alzheimer's disease on cerebral cortical anatomy: specificity and differential relationships with cognition. *NeuroImage*. 2013;76:332-344. doi:10.1016/j.neuroimage.2013.02.059
50. Latimer CS, Liachko NF. Tau and TDP-43 synergy: a novel therapeutic target for sporadic late-onset Alzheimer's disease. *GeroScience*. 2021. doi:10.1007/s11357-021-00407-0. Published online June 29.
51. de Flores R, Wisse LEM, Das SR, et al. Contribution of mixed pathology to medial temporal lobe atrophy in Alzheimer's disease. *Alzheimers Dement J Alzheimers Assoc*. 2020;16(6):843-852. doi:10.1002/alz.12079
52. Harper L, Bouwman F, Burton EJ, et al. Patterns of atrophy in pathologically confirmed dementias: a voxelwise analysis. *J Neurol Neurosurg Psychiatry*. 2017;88(11):908-916. doi:10.1136/jnnp-2016-314978

53. Huang W, Zhou Y, Tu L, et al. TDP-43: from Alzheimer's disease to limbic-predominant age-related TDP-43 encephalopathy. *Front Mol Neurosci*. 2020;13. doi:10.3389/fnmol.2020.00026
54. Latimer CS, Burke BT, Liachko NF, et al. Resistance and resilience to Alzheimer's disease pathology are associated with reduced cortical pTau and absence of limbic-predominant age-related TDP-43 encephalopathy in a community-based cohort. *Acta Neuropathol Commun*. 2019;7(9). doi:10.1186/s40478-019-0743-1
55. Bocancea DI, Svenningsson AL, van Loenhoud AC, et al. Determinants of cognitive and brain resilience to tau pathology: a longitudinal analysis. *Brain*. doi:10.1093/brain/awad100. Published online March 27, 2023:awad100.
56. Buckley RF, Scott MR, Jacobs HIL, et al. Sex mediates relationships between regional tau pathology and cognitive decline. *Ann Neurol*. 2020;88(5):921-932. doi:10.1002/ana.25878
57. Duong MT, Nasrallah IM, Wolk DA, Chang CCY, Chang TY. Cholesterol, atherosclerosis, and APOE in vascular contributions to cognitive impairment and dementia (VCID): potential mechanisms and therapy. *Front Aging Neurosci*. 2021;13:647990. doi:10.3389/fnagi.2021.647990
58. Neltner JH, Abner EL, Baker S, et al. Arteriolosclerosis that affects multiple brain regions is linked to hippocampal sclerosis of ageing. *Brain*. 2014;137(1):255-267. doi:10.1093/brain/awt318
59. Snyder HM, Corriveau RA, Craft S, et al. Vascular contributions to cognitive impairment and dementia including Alzheimer's disease. *Alzheimers Dement*. 2015;11(6):710-717. doi:10.1016/j.jalz.2014.10.008
60. Lin Z, Sur S, Liu P, et al. Blood-brain barrier breakdown in relationship to Alzheimer and vascular disease. *Ann Neurol*. 2021;90(2):227-238. doi:10.1002/ana.26134

SUPPORTING INFORMATION

Additional supporting information can be found online in the Supporting Information section at the end of this article.

How to cite this article: Lyu X, Duong MT, Xie L, et al. Tau-neurodegeneration mismatch reveals vulnerability and resilience to comorbidities in Alzheimer's continuum. *Alzheimer's Dement*. 2024;20:1586–1600. <https://doi.org/10.1002/alz.13559>